ATOM OPTICS AS A TESTING GROUND FOR QUANTUM CHAOS

C. F. BHARUCHA, J. C. ROBINSON [a], F. L. MOORE [b], K. W. MADISON,
S. R. WILKINSON, BALA SUNDARAM, AND M. G. RAIZEN
Department of Physics, The University of Texas at Austin,
Austin, TX 78712, USA

This paper summarizes our recent work on the role of classical dynamics in atom optics with time-dependent dipole potentials. We measure momentum transfer in parameter regimes for which the classical dynamics are chaotic and observe a wide range of phenomena. These include classical mechanisms such as the resonance overlap route to global chaos as well as quantum suppression due to dynamical localization. The high degree of experimental control enables detailed comparison with theory and opens up new avenues for testing ideas in quantum chaos.

1 Introduction

The past few years have seen a resurgence in the use of classical mechanics in the description of strongly perturbed and strongly coupled quantum systems in atomic physics [1,2], where the traditional perturbative treatment of the Schrödinger equation breaks down. In particular, recent advances in classical nonlinear dynamics and chaos have had important applications in the description of the photo-absorption spectrum of Rydberg atoms in strong magnetic fields [3], the microwave ionization of highly excited hydrogen atoms [4], and the excitation of doubly excited states of helium atoms [5]. These examples together with recent work on mesoscopic systems [6] explore classical-quantum correspondence in situations where the classical limit exhibits chaos, an area of study referred to as 'quantum chaos' [7].

Parallel progress in laser cooling and trapping techniques have led in recent years to spectacular advances in the manipulation and control of atomic motion [8]. At the ultra-cold temperatures that are now attainable, the wave nature of the atoms becomes important, leading to the development of the new field of atom optics [9].

Until recently, the primary focus in atom optics has been the development of optical elements such as atomic mirrors, beamsplitters and lenses for atomic de Broglie Waves. Our recent work, reviewed in this paper, has emphasized the novel regime of time-dependent potentials and hence dynamics in atom optics. In particular, we study momentum distributions of ultra-cold atoms exposed to time-dependent one-dimensional dipole forces which are, typically, highly nonlinear. Thus, the classical equations of motion can become chaotic and as dissipation can be made negligibly small in this system, quantum effects can become important. Our work has established that these features together make atom optics a very simple and controlled setting for the experimental study of quantum chaos [10].

As this work deals with momentum transfer from light to atoms, it is important to review some basic concepts. The relevant unit of momentum is one-photon recoil ($\hbar k_L$), the momentum change experienced by an atom when it scatters a photon. For sodium atoms, this velocity change is 3 cm/s. The desired process for atom optics is stimulated scattering, where the atom remains in the ground state, and

coherently scatters the photon in the direction of the laser beam. Spontaneous scattering, on the other hand, is a dissipative process and must be minimized. In a single beam (traveling wave) the atom scatters in the forward direction, and there is no net momentum transfer. However in a standing wave of light, created by the superposition of two counter-propagating beams, the atom can also back-scatter. This process leads to a momentum change of two photon recoils, or 6 cm/s velocity change for sodium. The effective dipole potential that the atom experiences scales with intensity I and detuning δ_L from atomic resonance as I/δ_L while spontaneous scattering goes as I/δ_L^2 [11]. Therefore, by detuning farther from resonance, it is possible to make the probability of spontaneous scattering negligible, while still having a substantial dipole potential.

2   Experimental method

The experimental study of momentum transfer in time-dependent interactions consists of three important components: initial conditions, interaction potential, and measurement of atomic momentum. The initial distribution should ideally be narrow in position and momentum, and should be sufficiently dilute so the atom- atom interactions can be neglected. The time-dependent potential should be one-dimensional (for simplicity), with full control over the amplitude and phase. In addition, noise must be minimized to enable the study of quantum effects. Finally the measurement of final momenta after the interaction should have high sensitivity and accuracy. Using techniques of laser cooling and trapping it is possible to realize all these conditions.

A schematic of the experimental set-up is shown in Fig. 1 [12,13]. Our initial conditions are a sample of ultra-cold sodium atoms which are trapped and laser-cooled in a magneto-optic trap (MOT) [8,14]. The atoms are contained in an ultra-high vacuum glass cell at room temperature. The cell is attached to a larger stainless steel chamber which includes a 20 l/s ion pump. The source of atoms is a small sodium ampoule contained in a copper tube that is attached to the chamber. The ampoule was crushed to expose the sodium to the rest of the chamber. Although the partial pressure of sodium at room temperature is below 10^{-10} Torr, there are enough atoms in the low-velocity tail of the velocity distribution that can be trapped. The trap is formed using three pairs of counter-propagating, circularly polarized laser beams (2.0 cm beam diameter) which intersect in the middle of the glass cell, together with a magnetic field gradient which is provided by current-carrying wires arranged in an anti-Helmholz configuration. This configuration is now fairly standard, and is used in many laboratories. These beams originate from a dye laser that is locked 20 MHz to the low frequency (red) side of the $(3S_{1/2}, F = 2) \longrightarrow (3P_{3/2}, F = 3)$ sodium transition at 589 nm. Approximately 10^5 atoms are trapped in a cloud which has an RMS size of 0.12 mm, with an RMS momentum spread of $4.6\hbar k_L$.

The interaction potential is provided by a second dye laser that is tuned typically 5 GHz red of resonance. Different beam configurations were used in the experiments described here utilizing acousto-optic and electro-optic modulators to control the time-dependent amplitude and phase.

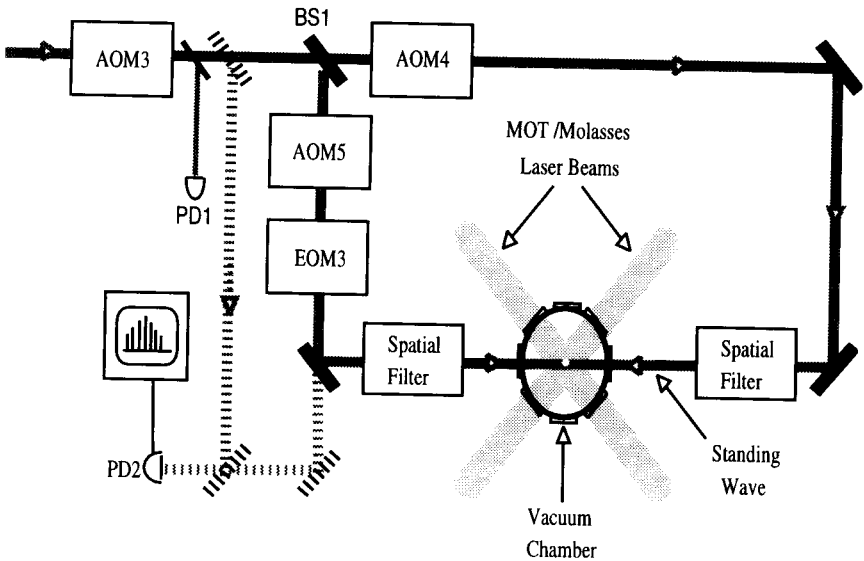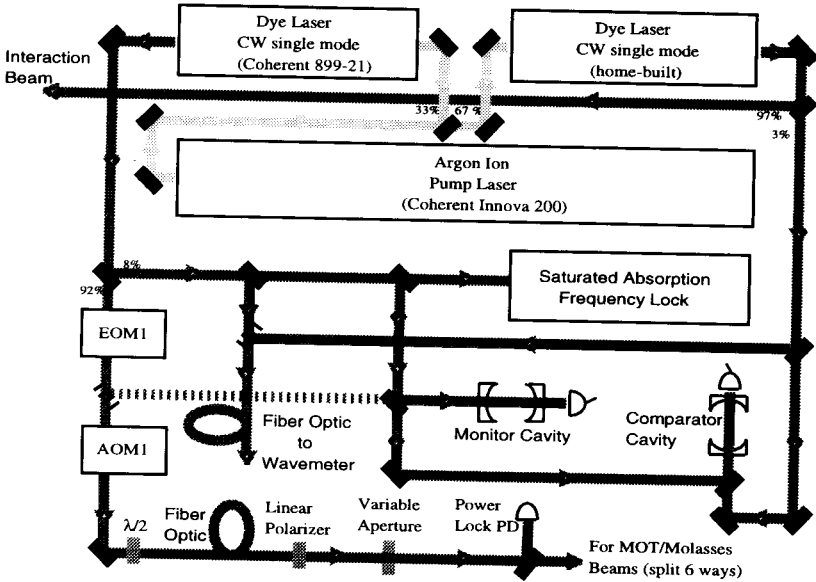The detection of momentum is accomplished by allowing the atoms to drift in

Figure 1: Schematic of the experiment. The upper part of the figure shows the laser set-up while the lower part shows the beam configuration in the modulated standing wave experiment. The acousto-optic modulators (AOM) are used for frequency shifts and as fast shutters while the electro-optic modulators (EOM) are used as phase shifters and frequency modulators.
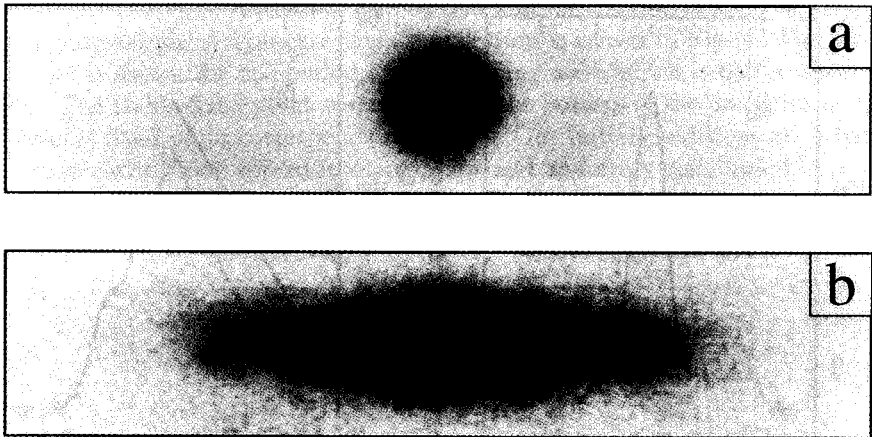
Figure 2: Two-dimensional atomic distributions after free expansion. (a) Initial thermal distribution with no interaction. (b) Localized distribution after interaction with the potential.

the dark for a controlled duration, after the interaction with the standing wave. Their motion is frozen by turning on the optical trapping beams in zero magnetic field to form optical molasses [8]. The motion of the atoms is overdamped, and for short times (tens of ms) their motion is negligible. The position of the atoms is then recorded via their fluorescence signal on a Charge Coupled Device (CCD) and the time of flight is used to convert position into momentum. The entire sequence of the experiment is computer controlled.

In Fig. 2, typical 2-D images of atomic fluorescence are shown. In Fig. 2(a) the initial MOT was released, and the motion was frozen after a 2 ms free-drift time. This enables a measurement of the initial momentum distribution. The distribution of momentum in Fig. 2(a) is Gaussian in both the horizontal and vertical directions. The vertical direction is integrated to give a one dimensional distribution as shown in Fig. 3(a). In Fig. 2(b), the atoms were exposed to a particular time dependent potential. The vertical distribution remains Gaussian, but the horizontal distribution becomes exponentially localized due to the interaction potential, as shown in Fig. 3(b). The significance of the lineshape and other characteristics are analyzed below.
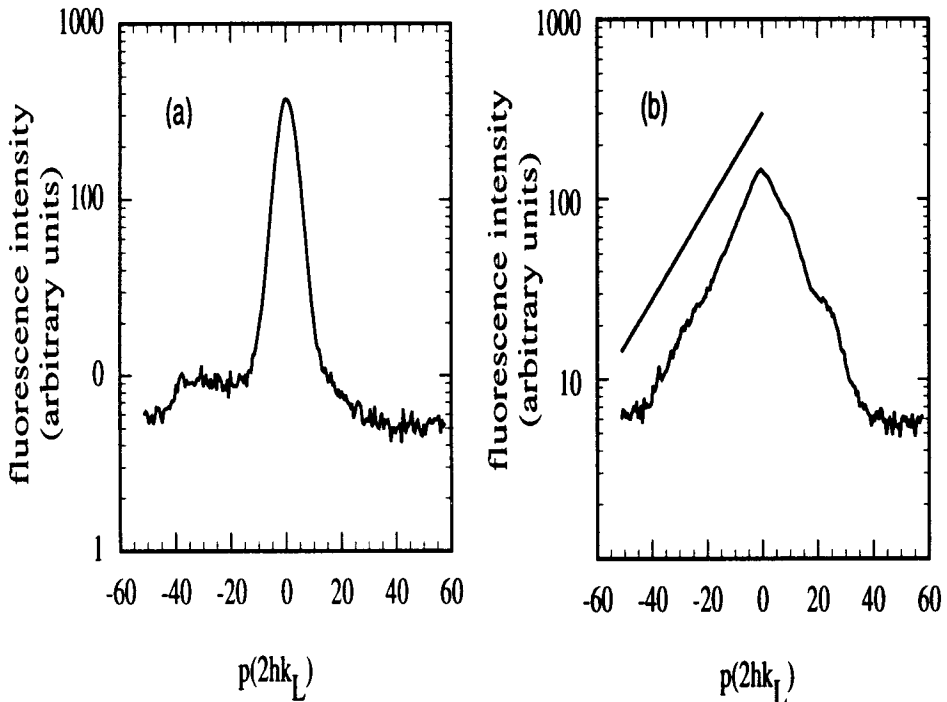
Figure 3: One-dimensional atomic momentum distributions. They were obtained by integrating along the vertical axes of the $2-D$ distributions in the previous figure. The horizontal axes are in units of two recoils, and the vertical axes show fluorescence intensity on a logarithmic scale. (a) Initial thermal distribution with no interaction. (b) Localized distribution after interaction with the potential. The significance of the characteristic exponential lineshape is discussed in the text.

3 Single Pulse Interaction

Consider a two level atom of transition frequency ω_0 interacting with a standing-wave of near-resonant light (frequency ω_L). For sufficiently large detuning $\delta_L = \omega_0 - \omega_L$, the excited state amplitude can be neglected and the atom remains in the ground state. The Hamiltonian is then given by

$$H = p^2/2M - (\hbar\Omega_{eff}/8)\cos 2k_L x \ , \tag{1}$$

where the effective Rabi frequency is $\Omega_{eff} = \Omega^2/\delta_L$, and k_L is the wavenumber. Ω_{eff} is proportional to the laser intensity I. The effective one-dimensional potential neglects variations of the potential in the two transverse directions. This is justified when the beams are sufficiently large compared to the initial atomic cloud. Quantum mechanically, the atom can exchange energy with the standing wave only in units of $2\hbar k_L$ which results in a ladder of equally spaced momentum states.

The classical analysis of this Hamiltonian is the same as for a pendulum, except

that here the conjugate variables are position and momentum instead of angle and angular momentum. A Poincaré surface of section is shown in Fig. 4. The position coordinate is shown for one period of the standing wave which is half a wavelength of light. The stable fixed point corresponds to the bottom of the potential well, and the unstable fixed point corresponds to the top. Our initial conditions are a band in phase space, with small spread in momentum, and uniformly distributed in position on the scale of one period.
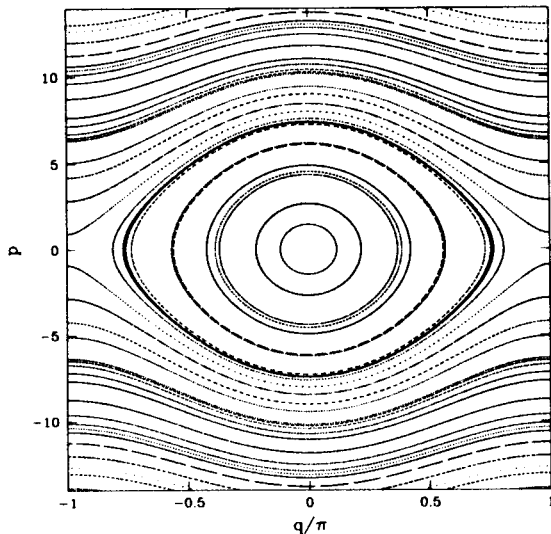

Figure 4: Poincaré surface of section for a single resonance. Momentum (vertical axis) is in units of two recoils, and position is in units of one period of the standing wave potential.

The simplest time-dependent potential is the turning on and off of an interaction, and one expects that for slow turn on/off the evolution will be adiabatic. The conditions for adiabatic behavior are usually very clear for linear potentials (the harmonic oscillator is an example) since there are only a few relevant time scales to consider. The difficulty with nonlinear potentials such as that occuring in the pendulum and the standing wave of light is that there are many time scales, so the conditions for adiabaticity must be examined much more carefully. The opposite extreme of fast passage is generally simpler to understand. We show that for time-scales intermediate to fast passage and adiabatic, mixed phase space dynamics and chaos can be seen even with the mere act of turning an interaction on and off. In the context of atom optics, this type of time-dependent interaction is ubiquitous and occurs, for example, whenever an atomic beam passes through a standing wave of light.

The generic time dependent potential in this case is

$$V(x,t) = (\hbar\Omega_{eff}/8)f(t)\cos 2k_L x \tag{2}$$

One common case is for $f(t) = \exp{-(t/\tau)^2}$ corresponding an atomic beam traversing a Gaussian beam waist [15]. We consider here the case $f(t) = \sin^2 \pi t/T_s$, which is turned on for a single period T_s.

This Hamiltonian can be expanded as

$$
\begin{aligned}
H &= p^2/2M - (\hbar\Omega_{eff}/8)\sin^2(\pi t/T_s)\cos(2k_Lx) , \\
&= p^2/2M - (\hbar\Omega_{eff}/16)[\cos 2k_Lx \\
&\quad - (\cos 2k_L(x - v_mt) + \cos 2k_L(x + v_mt))/2] ,
\end{aligned}
\tag{3}
$$

where $v_m = \lambda_L/2T_s$. The effective interaction is that of a stationary wave with two counter-propagating waves moving at $\pm v_m$. Classically, there are now three resonance zones each of width proportional to $\sqrt{\Omega_{eff}}$ and separation in momentum proportional to T_s^{-1}. The Poincaré surface of section for this Hamiltonian is shown in Fig. 5. Keeping Ω_{eff} constant and increasing T_s leads to the overlap of these isolated resonances and the subsequent diffusion of the particle in momentum. This is the well known Chirikov resonance overlap criterion for global chaos in Hamiltonian systems [16,17]. An example of a surface of section in that case is shown in Fig. 6. The parameters for resonance overlap are easily accessible experimentally [18].

To experimentally determine the threshold τ_{cr} for overlap, we must distinguish the momentum growth associated with spreading within the primary resonance from diffusion that can occur after resonance overlap. This is accomplished by contrasting the momentum transfer from the potential due to a standing wave of fixed amplitude

$$
V'(x) = (\hbar\Omega_{eff}/16)\cos(2k_Lx) ,
\tag{4}
$$

for duration T_s with

$$
\begin{aligned}
V(x,t) &= (\hbar\Omega_{eff}/16)[\cos 2k_Lx \\
&\quad - (\cos 2k_L(x - v_mt) + \cos 2k_L(x + v_mt))/2] ,
\end{aligned}
\tag{5}
$$

resulting from the sin^2 amplitude modulated standing wave. The key to the interpretation of the experimental results is the realization that *for values of T_s below the threshold for resonance overlap $V'(x)$ and $V(x,t)$ should give the same result*. After overlap of the resonances, $V(x,t)$ will result in significantly larger momentum transfer than $V'(x)$. The experimental results in Fig. 7(b) show the RMS momentum for both cases as a function of pulse duration (rise and fall times of 25 ns are included in the square pulse duration). These agree well with numerical classical simulations shown in Fig. 7(a) as well as with the estimated resonance overlap threshold [18].

How does the predicted quantum behavior compare with experiment and classical simulations? As seen from the dashed curve in Fig. 7(c), we find close agreement between all three for the square pulse potential $V'(x)$. This is an interesting result in its own right, since the coherent oscillations that occur for short times are seen in the experiment with a large ensemble of independent atoms, and in the quantum simulation which uses a single wavepacket approach. For the case of $V(x,t)$ there is also good agreement between the three cases over the entire range of pulse times. However, the quantum widths are slightly lower than the corresponding classical values near the large peak in the RMS width. Although this difference is too small
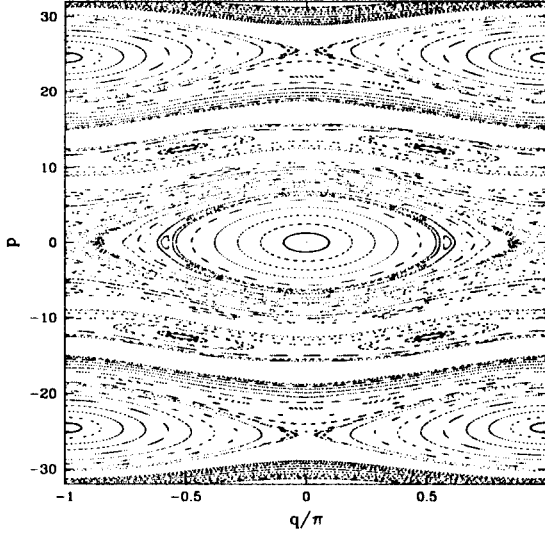
Figure 5: Poincaré surface of section for the sin^2 potential. In this case there are three isolated resonances at 0 and ±25.
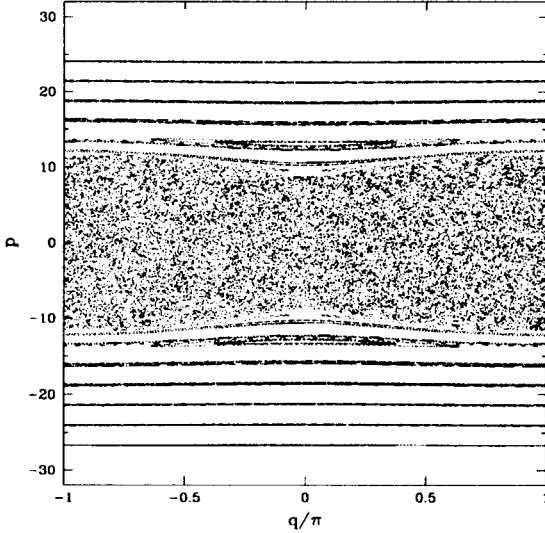

Figure 6: Poincaré surface of section for the sin^2 potential after resonance overlap has occured. There is a bounded region of global chaos.
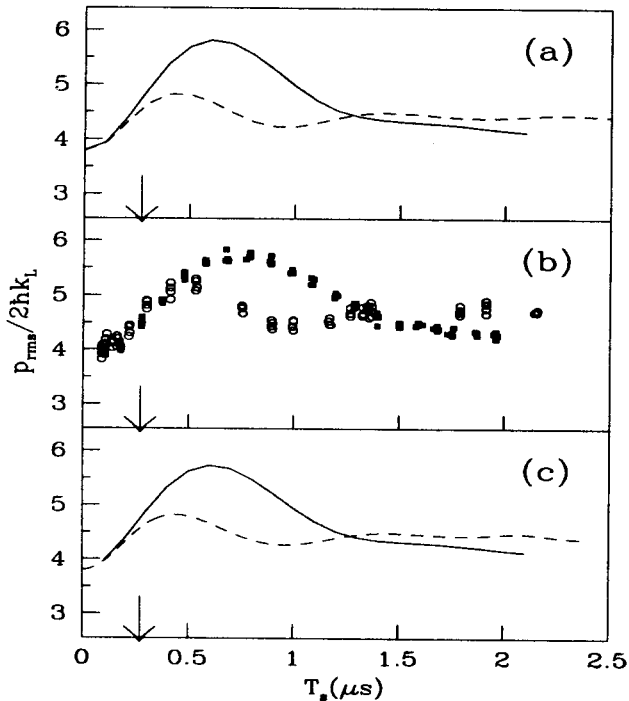
Figure 7: RMS momentum computed from (a) classical simulations for $\sin^2$ (solid line) and square (dashed line) pulses; (b) experimentally measured momentum distributions for $\sin^2$ (solid) and square (open) pulses (from Ref. 18); (c) corresponding quantum simulations, solid and dashed lines respectively. $\Omega_{eff}/2\pi = 41$MHz. and the threshold estimated from resonance overlap is indicated by the arrow. A clear deviation occurs at a pulse duration close to the predicted value.

to be of quantitative significance, it is nevertheless the precursor for differences in quantum and classical behavior that can occur when the classical dynamics are globally chaotic. These differences, which form the basis for the study of quantum chaos, are the focus of the next experiments we discuss.

4   Modulated Standing Wave

We now subject our two-level atoms to a standing wave of near-resonant light where the position of the nodes of the standing wave are modulated at an angular frequency ω_m and with an amplitude ΔL. Once again, a large detuning is used to eliminate the upper level dynamics leading to the effective Hamiltonian [19]

$$H = p^2/2M - (\hbar\Omega_{eff}/8)\cos\left[2k_L(x - \Delta L\sin\omega_m t)\right],\qquad(6)$$

Although this Hamiltonian may look somewhat different than the sin^2 case that was discussed earlier, it can also be expanded as a sum of nonlinear resonances using

the well known Bessel function expansion. The Hamiltonian then has the form

$$
\begin{aligned}
V(x,t) &= (\hbar\Omega_{eff}/8)\left[J_0(\lambda)\cos(2k_Lx) + J_1(\lambda)\cos 2k_L(x - v_mt)\right. \\
&+ \left. J_{-1}(\lambda)\cos 2k_L(x + v_mt) + J_2(\lambda)\cos 2k_L(x - 2v_mt)\cdots\right] \\
&= (\hbar\Omega_{eff}/8)\sum_{m=-\infty}^{\infty} J_m(\lambda)\cos 2k_L(x - mv_mt) ,
\end{aligned}
\tag{7}
$$

where J_m are ordinary Bessel functions and $v_m = \omega_m/2k_L$. $\lambda = 2k_L\Delta L$ is the control parameter which takes the dynamics from integrable ($\lambda = 0$) to chaotic. Unlike the single pulse case that was considered earlier, here we take the interaction time to be independent of the modulation period.

Now the classical dynamics involves several resonances equally spaced in momentum with widths proportional to $\sqrt{|J_m(\lambda)|}$. For a given value of λ there are substantial resonances only for $m \leq \lambda$ therefore the interaction turns off for $v > \lambda v_m$, leading to a bounded region in momentum spanned by the resonances. The oscillatory behavior of the Bessel functions leads to the recurrence of stable classical structures within a bounded region of chaos, as λ is varied.

The classical dynamics can also be understood in terms of resonant-kicks that occur twice during each modulation period: consider an atom subjected to the modulated standing wave. When the standing wave is moving with respect to the atom, the time-averaged force is zero, since the sign of the force is changing as the atom goes over 'hill and dale' of the periodic potential. However, twice during each modulation period, the standing wave is stationary in the rest frame of the atom, and the atom gets a resonant-kick which changes its momentum. The magnitude and direction of the resonant-kick depends on where the atom is located with respect to the standing wave at that time. In this system, an atom experiences two resonant-kicks every modulation period, although they are not equally spaced in time. The boundary in momentum can be understood from this picture, since for each value of λ there is a maximum velocity of the standing wave. Once an atom is moving faster than this maximum valocity, the resonant-kicks cannot occur, and the atom is essentially free.

The variation of the classical RMS momentum width as a function of λ is shown in Fig. 8 (dot-dashed line)[20]. The parameters are $\omega_m/2\pi = 1.3$ MHz. and $\Omega_{eff}/2\pi \approx 25$ MHz.. The interaction time was chosen to be 20 μs which is sufficiently long for the experimentally observed momentum spread to saturate. At small values of λ, the distribution of the classical simulation saturates near the resonant-kick boundary. As λ is increased, oscillations occur with the dips corresponding to zeros of the Bessel functions. Notice that the overall amplitude of the oscillations decreases as λ is increased due to the reduction of the size of each resonant-kick. This can be understood from the impulse approximation, since the maximum classical force is fixed, but the time that the standing wave potential is stationary in the rest frame of the atom is inversely proportional to λ. We have run the classical simulation for longer times and find that the peaks grow until the resonant-kick boundary, while the dips grow much more slowly. This difference in rates is explained by the phase portraits shown in Fig. 9 (top panel). In this figure, the peaks in RMS momentum are at values of λ for which the dynamics are primarily chaotic. In contrast, at the dips, a
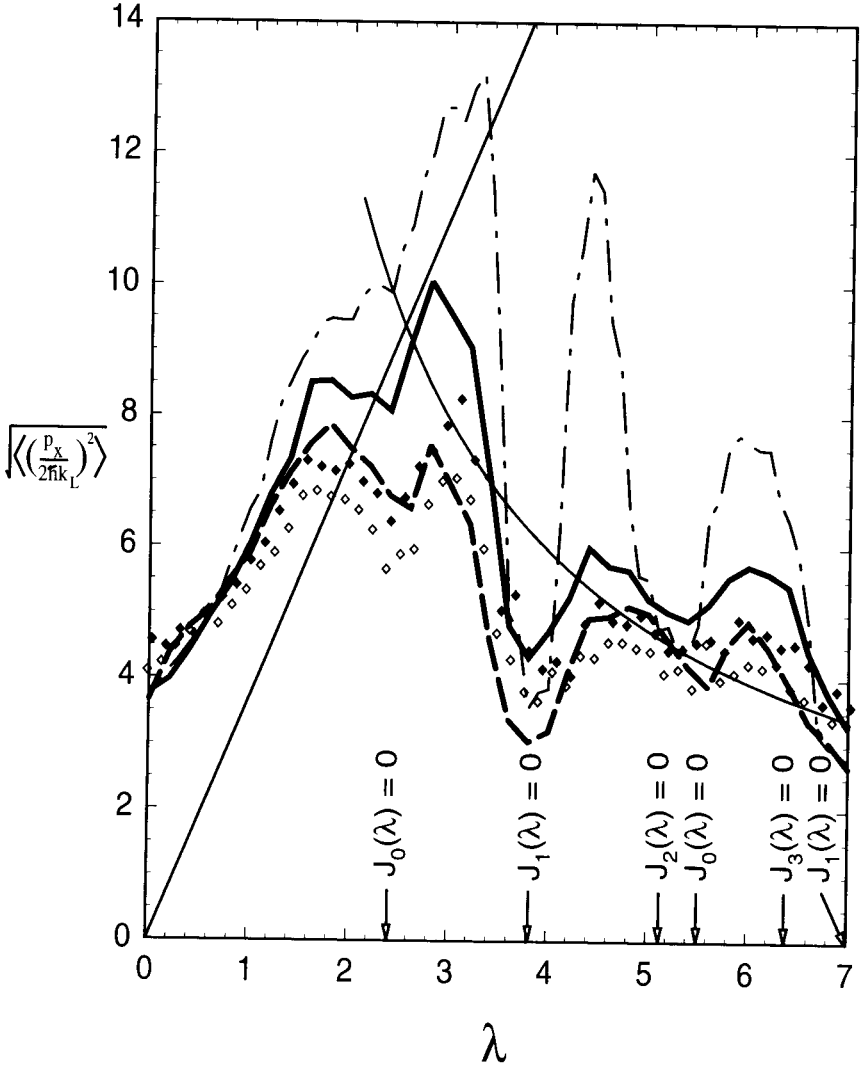
Figure 8: The RMS momentum width as a function of the modulation amplitude λ. Experimental data is denoted by diamonds and have a 10% uncertainty associated with them. The empty diamonds are for an interaction time of 10 μs and the solid diamonds are for 20 μs; classical simulation for 20 μs (dash-dot line); quantum Schrödinger for 20 μs (heavy dashed line); quantum Floquet in the long-time limit (heavy solid line). The light solid lines denote the resonant-kick boundary and the curve proportional to λ^{-1} predicted in Ref. 19.

primary island determines the momentum transfer. The classical lineshapes in Fig. 9 (middle panel) clearly show these features as well as the effect of the resonant-kick boundary. Initial conditions contained within an island remain trapped, while those in the chaotic domain diffuse up to the boundary, leading to 'boxlike' distributions. A clear example of the stability at the dips is at $\lambda = 3.8$ where J_1 has its first zero. The final momentum spread in this case is governed by the surviving island due to J_0 and the system is nearly integrable. Note that the oscillations of the Bessel functions are reflected in the exchange of the location of hyperbolic and elliptic fixed points, which is clearly visible on contrasting the phase portraits for $\lambda = 0$ and $\lambda = 3.0$, beyond the first zero of J_0 at $\lambda = 2.41$.
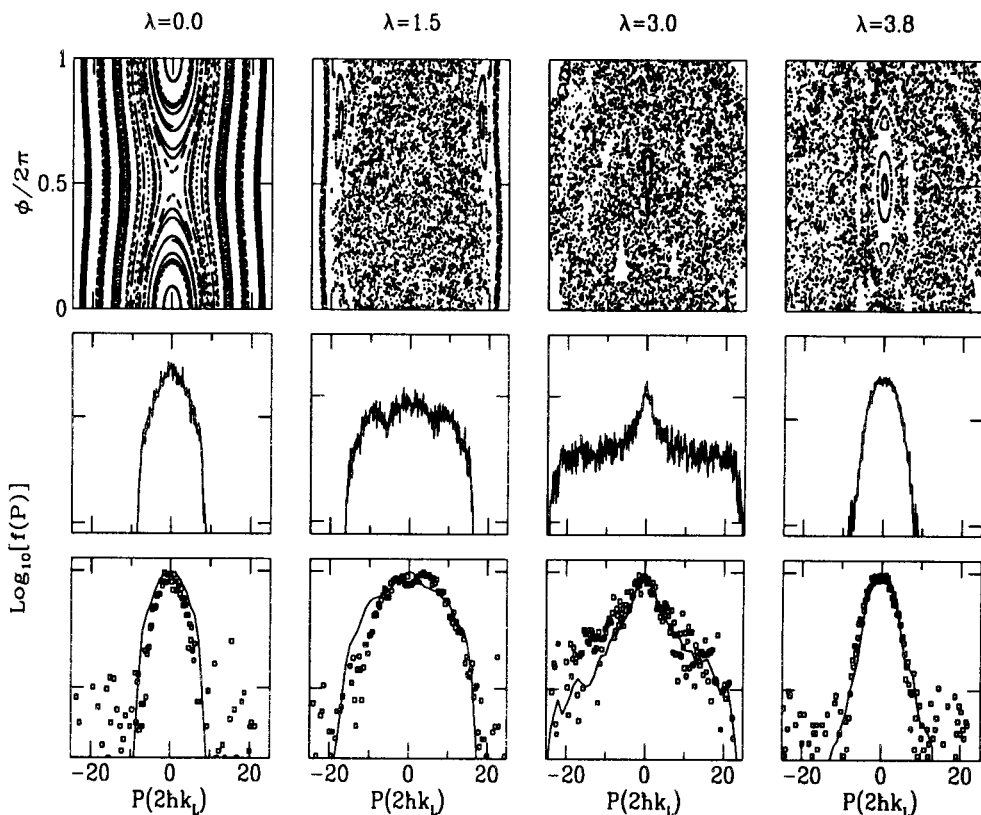

Figure 9: Poincaré surfaces of section (upper panel), classical momentum distributions (middle panel), and experimentally measured momentum distributions with Floquet theory (bottom panel, theory marked by lines) for runs with parameters similar to those in Fig. 8. Note that the vertical scales for the distributions are logarithmic and are marked in decades.

It is well known that classically diffusive behavior can be suppressed quantum mechanically by a mechanism analogous to Anderson localization [21]. Referred to as dynamical localization, it predicts saturation in the energy transfer (momentum,

in our case) and a resulting exponential lineshape with a characteristic localization length ξ (in momentum). In the experiments, we have to ensure that the location of the resonant-kick boundary is much further than ξ to observe this lineshape. As this boundary scales linearly with λ, we expect to see the appearance of dynamical localization only beyond some value of λ.

The measured RMS momenta vs. λ are shown in Fig. 8 (diamonds). The empty and solid diamonds are for two different interaction times showing that these results are close to saturation for the range of λ shown. Note that for small values of λ there is good agreement with the classical prediction. At $\lambda = 0$ the system is integrable and momentum is trivially localized. As λ is increased the phase space becomes chaotic, but growth is limited by the resonant-kick boundary. Our measured momentum distributions (in Fig. 9, bottom panel) are characteristically "boxlike" in this regime. As λ is increased beyond a critical value there are oscillations in localization with an RMS spread that deviates substantially from the classical prediction at the peaks. For those values of λ the classical phase space is predominately chaotic, and exponentially localized distributions are observed [13,20]. This is shown in Fig. 9 for $\lambda = 3.0$. At the dips in oscillation, as in the case $\lambda = 3.8$, the classical phase space becomes nearly integrable and the measured momentum is close to the classical prediction.

Quantum analyses under the conditions of the experiment as well as an asymptotic (long-time limit) Floquet analysis are also shown in Fig. 8 as are the predicted lineshapes in lower panel of Fig. 9. It is clear that there is good quantitative agreement between experiment and the effective single particle analysis [20,22].

The modulated system is characterized in general by a mixed phase space. In certain regimes such as for $\lambda = 3.0$, the stable regions become very small, and dynamical localization can be observed. The main potential for future work with the modulated system is, however, the study of quantum dynamics in a mixed phase space. This will require better defined initial conditions that are localized in position as well as momentum, and will be the main emphasis of a cesium experiment that is now being contructed in our laboratory.

Mixed phase space dynamics inherently complicate the analysis of dynamical localization and it is useful to realize a system where the chaos is more widespread. Also, there is a characteristic time scale, the 'quantum break time', beyond which the saturation effects of dynamical localization are predicted to occur. With a further modification of the basic experimental setup, we can achieve both the globally chaotic behavior as well as the capability to track the time evolution of the localization phenomena.

5 Kicked Rotor

The classical kicked rotor or the equivalent standard mapping is a textbook paradigm for Hamiltonian chaos. The Hamiltonian for the problem is given by

$$H = p^2/2 + K \cos q \sum_n \delta(t - nT) \tag{8}$$

The evolution consists of resonant-kicks that are equally spaced in time, with free motion in betwen. K is called the stochasticity parameter, and is the standard control parameter. As K is increased, the size of each resonant- kick grows. Beyond a threshold value of $K = 4$ it was shown that phase space is globally chaotic [21]. The quantum version of this problem has played an equally important role for the field of quantum chaos, and a wide range of effects have been predicted [21]. In our realization, we have the cosine potential of the standing wave multiplied by $f(t)$, a train of N pulses with unit peak heights and period T. This system was previously analyzed in the context of molecular rotation excitation [23]. The nonzero pulse widths lead to a finite number of resonances in the classical dynamics,which limits the diffusion resulting from overlapping resonances to a band in momentum. However, by decreasing the pulse duration with constant area, the width of this band can be made arbitrarily large, approaching the δ- function pulse limit. The boundary in momentum can also be understood using the concept of an impulse. If the atomic motion is negligible while the pulse is on, the momentum transfer is an impulse, similar to the resonant-kick in the modulated system. For a sufficiently large velocity, the atom has time to move over the periodic potential while the pulse is on, averaging the impulse to zero. The result is a momentum boundary which can be pushed out by making each pulse shorter. The practical constraints of available laser power limits the pulse duration, since in these experiments the pulse train is created by turning a continuous-wave laser on and off with an acousto-optic modulator.
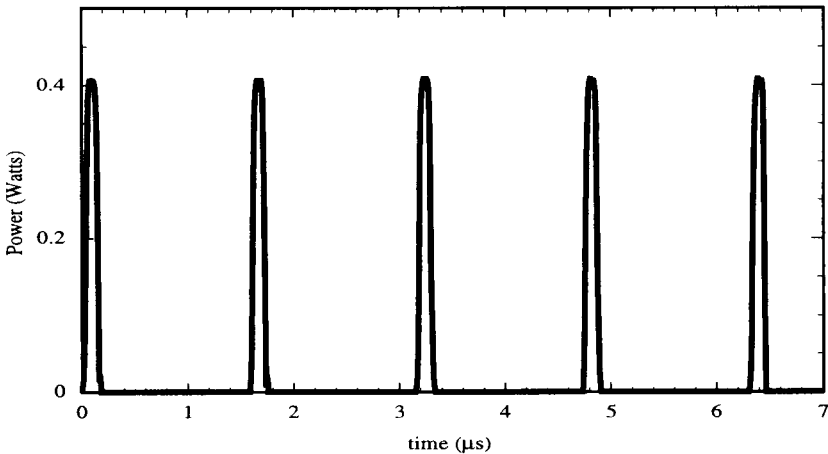

Figure 10: Digitized temporal profile of the pulse train measured on a fast photo-diode. The vertical axis represents the total power in both beams of the standing wave. $f(t)$ and Ω_{eff} are derived from this scan.

A typical experimental pulse train is shown in Fig. 10. Each pulse is typically non-Gaussian and the integrated area is used in the comparison with theory. The pulse period, duration, and number of pulses in a burst are variable parameters in the experiment. The bounded region of chaos arising from the finite pulse duration

is illustrated by the classical phase portrait, for typical experimental parameters, shown in Fig. 11. The central region of momentum in this phase portrait is in very close agreement with the delta-kicked rotor model with a stochasticity parameter of $K = 11.6$, which is well beyond the threshold for global chaos.
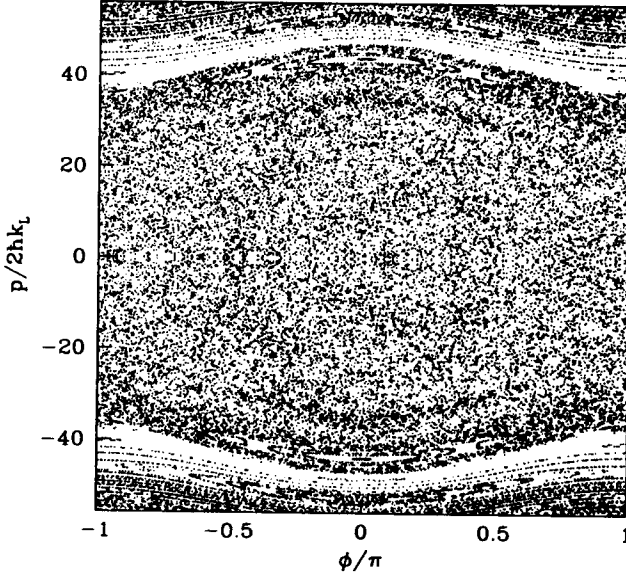

Figure 11: Poincaré surface of section for the pulsed system using a train of Gaussians to represent the experimental sequence. The integrated area under a single pulse is taken to be the same as in the experiment. The standing wave has a spatial RMS value of $\Omega_{eff}/2\pi = 75.6$ MHz. $T = 1.58 \,\mu s$, and $K = 11.6$.

The momentum distributions were measured for an increasing number of kicks (N), with the pulse height, period, and pulse duration fixed. This sequence of measurements then determines the temporal evolution. The lineshapes shown in Fig. 12 clearly evolve from an initial Gaussian distribution at $N = 0$ to an exponentially localized distribution after approximately $N = 8$. We have measured distributions out until $N = 50$ and find no further significant change. The growth of the mean kinetic energy of the atoms as a function of the number of kicks was calculated from the data and is displayed in Fig. 13. It shows diffusive growth initially until the quantum break time, after which dynamical localization is observed[24]. Though not shown here, classical and quantum calculations both agree with the data over the diffusive regime. Beyond the quantum break time, the classical energy continues to increase diffusively while the measured lineshapes stop growing, in agreement with
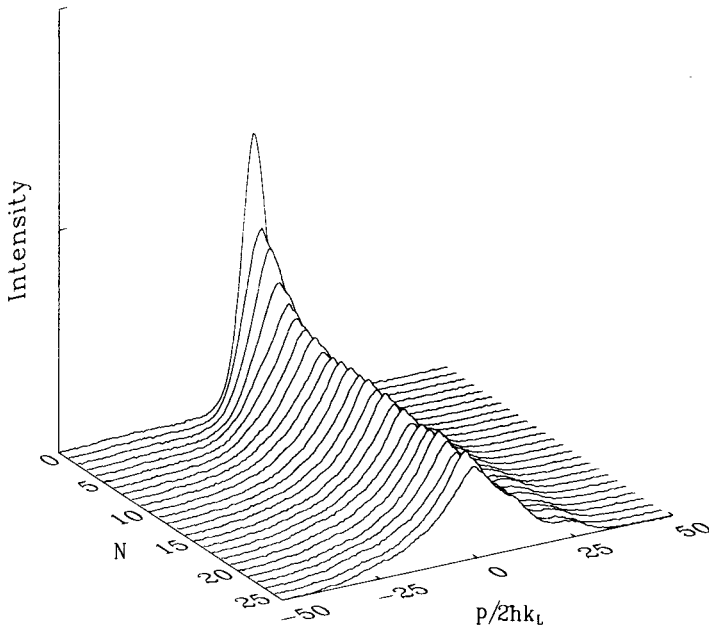
Figure 12: Experimental time evolution of the lineshape from the initial Gaussian until the exponentially localized lineshape (from Ref. 24). The break time is approximately 8 kicks. Fringes in the freezing molasses lead to small asymmetries in some of the measured momentum lineshapes as seen here and in the inset of Fig. 13. The vertical scale is measured in arbitrary units and is linear.

the quantum prediction. The observed lineshape is shown (Fig. 13 inset), and is clearly exponential. These results are the first experimental observation of the onset of dynamical localization in time, and the quantum break time [24].

Between kicks the atoms undergo free evolution for a fixed duration. The quantum phase accumulated during the free evolution is $e^{-ip^2T/2M\hbar}$. An initial plane wave at $p = 0$ couples to a ladder of states separated by $2\hbar k_L$. For particular pulse periods, the quantum phase for each state in the ladder is a multiple of 2π, a condition known as a *quantum resonance* [21]. More generally, a quantum resonance is predicted when the accumulated phase between kicks is a rational multiple of 2π. We have scanned T from 3.3 μs to 50 μs and find quantum resonances when the quantum phase is an integer multiple of π. For even multiples, the free evolution factor between kicks is unity, and for odd multiples, there is a flipping of sign between each kick. Quantum resonances have been studied theoretically, and it was shown that instead of localization, one expects energy to grow quadratically with time [25]. This picture, however, is only true for an initial plane wave. A general analysis of the quantum resonances shows that for an initial Gaussian wavepacket, or for narrow distributions not centered at $p = 0$, the momentum distribution is actually smaller than the exponentially localized one, and settles in after a few kicks [26]. Our experimental results are shown in Fig. 14. Ten quantum resonances are found for T ranging between 5 μs (corresponding to a phase shift of π) and 50 μs (10π) in steps of 5 μs. The saturated momentum lineshapes as a function of T are shown in Fig. 14(a). The narrower, non-exponential profiles are the resonances between
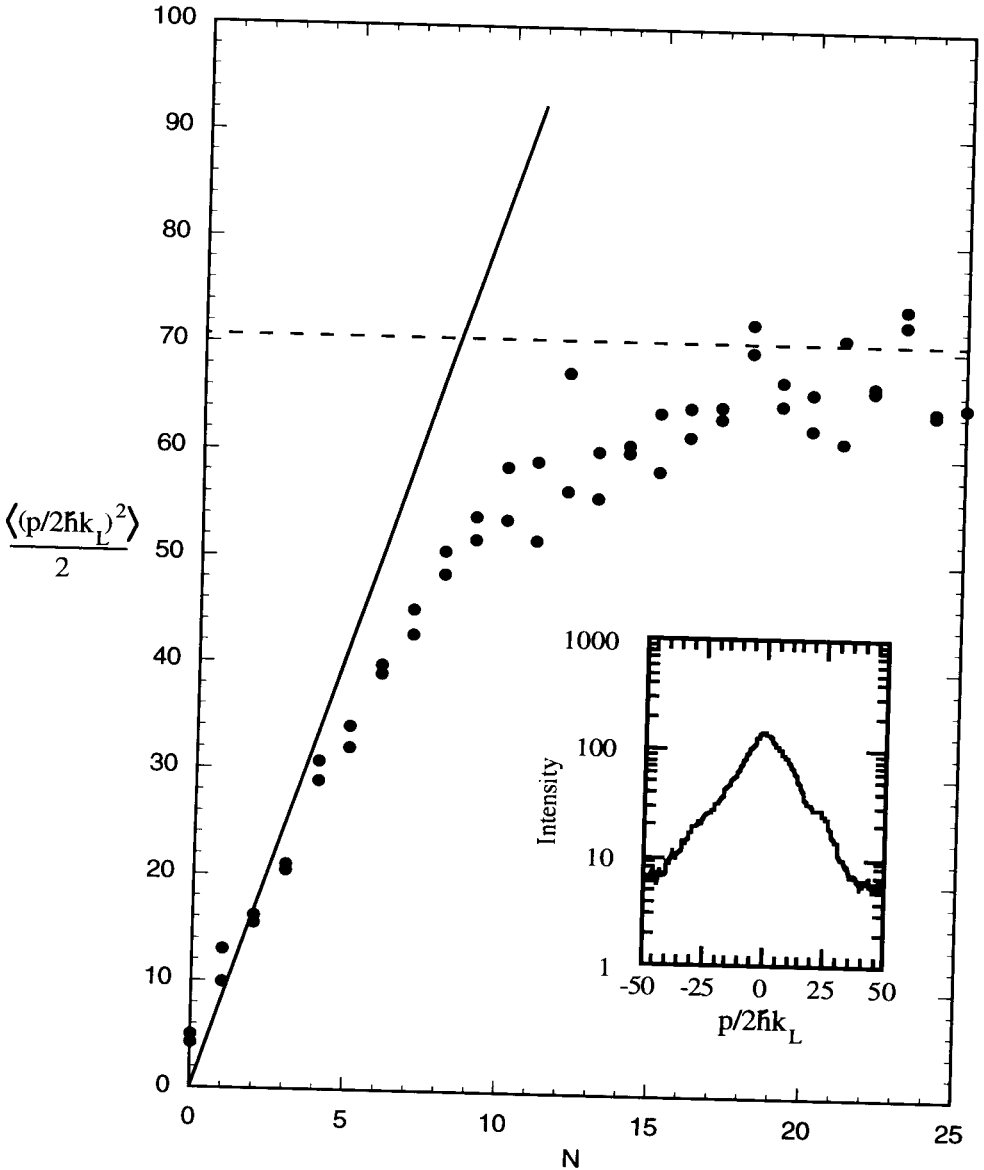
Figure 13: Energy $< (p/2\hbar k_L)^2 > /2$ as a function of time (from Ref. 24). The solid dots are the experimental results. The solid line shows the calculated linear growth from the classical dynamics. The dashed line is the saturation value computed from the theoretical localization length ξ. The inset shows an experimentally measured exponential lineshape on a logarithmic scale which is consistent with the theoretical prediction.
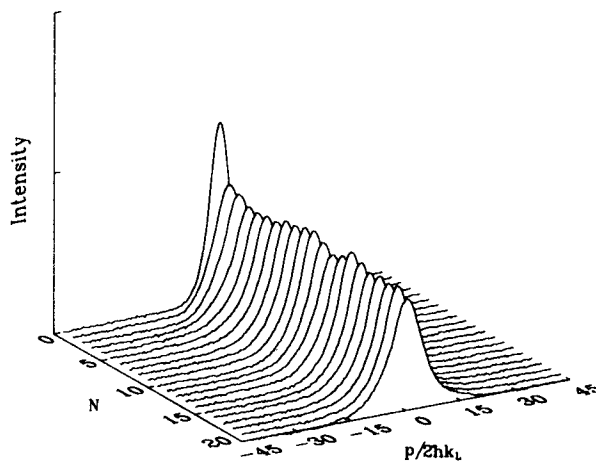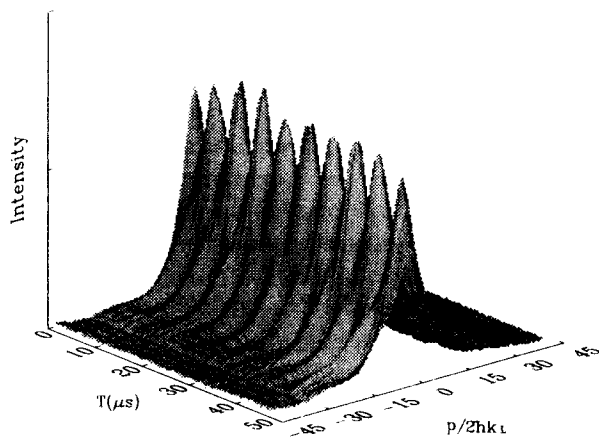
Figure 14: Experimental observation of quantum resonances: (a) Occurrence as a function of the period of the pulses. The surface plot is constructed from 150 lineshapes measured, for each T, after 25 kicks. This value of N ensures that the lineshapes are saturated for the entire range of T shown. At resonance, the profiles are non-exponential and narrower than the localized shapes which appear off-resonance. Note that the vertical scale is linear. (b) Time evolution of a particular resonance ($T = 10$ μs).

which the exponentially localized profiles are recovered. The time evolution of the lineshape at a particular resonance is shown in Fig. 14(b) from which it is clear that the distribution saturates after very few kicks.

6 Future Directions

This work establishes a new experimental testing ground for quantum chaos, and it should be possible to study many aspects of this field. These include the study of noise-induced delocalization[27,28] and localization in two and three dimensions[29]. Using recently developed techniques of atom cooling and manipulation it should be possible to prepare the atoms in a small region of phase space. This would enable a detailed study of quantum transport in mixed phase space. Some interesting topics to study would be tunneling from islands of stability, chaos assisted tunneling, and quantum scars[30].

[a] present address: Motorola, Semiconductor Technologies Laboratory, Austin, Texas 78721.
[b] present address: NOAA/CMDL, Nitrous Oxide and Halocompounds Division, Mail Stop R/E/CG1, Boulder, Colorado 80303.

References

1. *Irregular Atomic Systems and Quantum Chaos*, edited by J. C. Gay (Gordon and Breach, New York, 1992).
2. R. V. Jensen, *Nature* (London) **355**, 311 (1992).
3. H. Friedrich and D. Wintgen, *Phys.Reps.* **183**, 37 (1989); D. Delande in *Chaos and Quantum Physics*, eds. M.-J. Giannoni, A. Voros and J. Zinn-Justin (Elsevier, London, 1991).
4. P. M. Koch, and K. A. H. van Leeuwen, *Phys.Reps.* **255**, 289 (1995).
5. G. S. Ezra, K. Richter, G. Tanner and D. Wintgen, *J.Phys.* B24, L413 (1991).
6. see, for example, contibutions in *Physica* **D 83** (1995).
7. see, for example, *Quantum chaos : between order and disorder : a selection of papers*, edited by G. Casati and B. V. Chirirov (Cambridge Univ Press, New York, 1995).
8. Laser cooling and trapping is reviewed by Steven Chu in *Science* **253**, 861 (1991).
9. C. S. Adams, M. Sigel, and J. Mlynek, *Phys. Reps.* **240**, 145 (1994).
10. This work was reviewed in "Search and Discovery", *Physics Today* June 1995, pg. 18.
11. C. Cohen-Tannoudji, in *Fundamental Systems in Quantum Optics*, Les Houches, 1990; J. Dalibard, J. M. Raimond and J. Zinn-Justin, eds., (Elsevier, 1992).

12. J. C. Robinson, Ph.D. thesis, University of Texas at Austin, 1995 (University Microfilms, Ann Arbor, Michigan).
13. F. L. Moore, J. C. Robinson, C. Bharucha, P. E. Williams, and M. G. Raizen, *Phys. Rev. Lett.* **73**, 2974 (1994).
14. E. Raab, M. Prentiss, A. Cable, S. Chu, and D. Pritchard, *Phys. Rev. Lett.* **59**, 2631 (1987).
15. see, for example, P. J. Martin, P. L. Gould, B. G. Oldaker, A. H. Miklich, and D. E. Pritchard, *Phys. Rev.* **A36**, 2495 (1987).
16. B. V. Chirikov, *Phys. Reps.* **52**, 265 (1979).
17. G. H. Walker, and J. Ford, *Phys. Rev.* **188**, 416 (1969).
18. J. C. Robinson, C. F. Bharucha, K. W. Madison, F. L. Moore, Bala Sundaram, S. R. Wilkinson, and M. G. Raizen, *Phys. Rev. Lett.* **76**, 3304 (1996).
19. R. Graham, M. Schlautmann, and P. Zoller, *Phys. Rev.* **A45**, R19 (1992).
20. J. C. Robinson, C. Bharucha, F. L. Moore, R. Jahnke, G. A. Georgakis, Q. Niu, M. G. Raizen, and Bala Sundaram, *Phys. Rev. Lett.* **74**, 3963 (1995).
21. L. E. Reichl, *The Transition to Chaos in Conservative Classical Systems: Quantum Manifestations* Springer-Verlag (1992).
22. P. J. Bardroff, I. Bialynicki-Birula, D. S. Krähmer, G. Kurizki, E. Mayr, P. Stifter, and W. P. Schleich, *Phys. Rev. Lett.* **74**,3959 (1995).
23. R. Blümel, S. Fishman, and U. Smilansky, *J. Chem. Phys.* **84**, 2604 (1986).
24. F. L. Moore, J. C. Robinson, C. F. Bharucha, Bala Sundaram, and M. G. Raizen, *Phys. Rev. Lett.* **75**, 4598 (1995).
25. F. M. Izrailev, and D. L. Shepelyansky, *Sov. Phys. Dokl.* **24**, 996 (1979); *Theor. Math. Phys.* **43**, 553 (1980).
26. Q. Niu and Bala Sundaram, to be submitted for publication.
27. T. Dittrich and R. Graham, *Europhys. Lett.* **4**, 263 (1987).
28. S. Fishman, and D. L. Shepelyansky, *Europhys. Lett.* **16**, 643 (1991).
29. Giulio Casati, Italo Guarneri, and D. L. Shepelynansky, *Phys. Rev. Lett.* **62**, 345 (1989).
30. E. J. Heller, and S. Tomsovic, *Physics Today* **46**, 38 (1993).